International Journal of Modern Physics E


# Elliptic flow measurements of strange and multi-strange hadrons in isobar collisions at RHIC

V. Bairathi (for the STAR Collaboration)

*Instituto de Alta Investigación, Universidad de Tarapacá,*
*Arica 1000000, Chile*
*vipul.bairathi@gmail.com*

We present measurements of elliptic flow ($v_2$) of $K_s^0$, $\Lambda$, $\bar{\Lambda}$, $\phi$, $\Xi^-$, $\overline{\Xi}^+$, and $\Omega^-+\overline{\Omega}^+$ at mid-rapidity ($|\eta| < 1.0$) in isobar collisions ($^{96}_{44}$Ru+$^{96}_{44}$Ru and $^{96}_{40}$Zr+$^{96}_{40}$Zr) at $\sqrt{s_{\rm NN}}$ = 200 GeV by STAR. The centrality and transverse momentum ($p_{\rm T}$) dependence of elliptic flow are presented and the number of constituent quark (NCQ) scaling of $v_2$ in isobar collisions is discussed. The $p_T$-integrated elliptic flow ($\langle v_2\rangle$) is observed to increase from central to peripheral collisions. The ratio of $\langle v_2\rangle$ between the two isobars shows a deviation from unity for strange hadrons ($K_s^0$, $\Lambda$ and $\bar{\Lambda}$), suggesting differences in nuclear structure and deformation between the systems. Additionally, a dependency of the strange hadron $v_2$ on the system size at high $p_T$ is observed across various collision systems, including Ru+Ru, Zr+Zr, Cu+Cu, Au+Au, and U+U. A multi-phase transport (AMPT) model with string melting (SM) describes the experimental data well in the measured $p_{\rm T}$ range for isobar collisions at $\sqrt{s_{\rm NN}}$ = 200 GeV.

*Keywords*: Heavy-ion collisions; Isobar; Elliptic flow.

PACS numbers: 25.75.Ld

## 1. Introduction

Quantum chromodynamics (QCD), the theory that describes the strong interaction, predicts the existence of a matter with de-confined state of quarks and gluons known as quark-gluon plasma (QGP) under conditions of sufficiently high temperature and energy density.[1–3] Numerous experimental endeavors, particularly through heavy-ion collision experiments at both the Relativistic Heavy Ion Collider (RHIC)[4–7] and the Large Hadron Collider (LHC),[8–10] have provided evidence supporting the presence of the QGP. These experiments have been pivotal in exploring the partonic phase of matter, thereby significantly advancing our understanding of QCD in extreme conditions.

The collective flow, an observable reflecting the hydrodynamic behavior of the quark-gluon plasma, is analyzed through the Fourier expansion of the azimuthal angle distribution of emitted particles relative to the symmetry planes.[11] This azimuthal anisotropy in particle emission is indicative of the collective and hydrodynamic nature of the matter under extreme conditions.[12] It originates from the spatial anisotropy present in the initial geometry of the colliding nuclei, which is transformed into momentum anisotropy of the final state particles due to the dynamic evolution of the medium and interactions among the constituent partons.

The STAR experiment at RHIC collected data in the year 2018 by colliding isobars (Ru+Ru and Zr+Zr) at $\sqrt{s_{\rm NN}} = 200$ GeV. It was primarily aimed at exploring the charge separation phenomenon along the magnetic field, a process known as the Chiral Magnetic Effect (CME).[13] The two isobar nuclei have the identical atomic mass number but distinct nuclear deformation parameters. Collective flow measurements are highly sensitive to these parameters. Furthermore, the analysis is extended to the flow of strange and multi-strange hadrons. These particles serve as an excellent probe for understanding the initial state anisotropies due to their smaller hadronic interaction cross-section compared to light hadrons. Therefore, a systematic study of the anisotropic flow of strange and multi-strange hadrons could providing valuable insights on the effect of initial states in the isobar collisions.

## 2. Analysis details

In these proceedings, we report $v_2$ of $K_s^0$, $\Lambda$, $\bar{\Lambda}$, $\phi$, $\Xi^-$, $\overline{\Xi}^+$, and $\Omega^-$+$\overline{\Omega}^+$ at mid-rapidity ($|\eta| < 1.0$) in Ru+Ru and Zr+Zr collisions at $\sqrt{s_{\rm NN}} = 200$ GeV. The charged particle tracks are identified by the Time Projection Chamber (TPC) and Time of Flight (TOF) detector of the STAR. The particles are reconstructed using the invariant mass technique through their hadronic decay channels. The combinatorial background is constructed using a rotational method for weakly decaying hadrons, while for $\phi$-mesons event mixing technique is used.[14,15] The $\eta$-sub event plane method with a $\eta$-gap of 0.1 between the two sub-events (A: -1.0 $< \eta <$ -0.05 and B: 0.05 $< \eta <$ 1.0) is used to calculate $v_2$ of these hadrons.[11] The second-order Fourier coefficient $v_2$, known as elliptic flow, is particularly sensitive to the initial geometry of the collisions and the properties of the medium in the heavy-ion collisions. The event plane angle $\psi_n$ represents the orientation of the $n^{th}$-order event plane. It is obtained from the azimuthal distribution of final-state particles as,

$$\psi_n = \frac{1}{n}\tan^{-1}\frac{\sum_i w_i sin(n\phi_i)}{\sum_i w_i \cos(n\phi_i)}, \qquad (1)$$

where, $\phi_i$ and $w_i$ represent azimuthal angle and weight for the $i^{th}$ particle, respectively. The transverse momentum of a track is taken as weight $w_i$. In order to minimize the effects of non-flow correlations, charged particle tracks from TPC with a transverse momentum range of $0.2 < p_{\rm T} < 2.0$ GeV/$c$ are selected to reconstruct the event plane angle. Since the event plane angle is estimated using finite number of particles, flow coefficients need to be corrected for the event plane resolution. Therefore, the $v_2$ measured with respect to the reconstructed event plane is divided by the event plane angle resolution to get the final flow coefficients as,

$$v_2 = \frac{v_2^{obs}}{\sqrt{\left\langle \cos\left[2(\psi_2^A - \psi_2^B)\right]\right\rangle}}. \qquad (2)$$

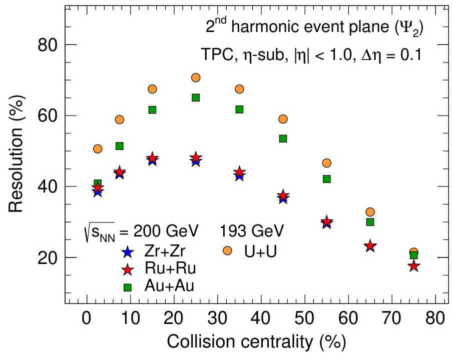


Fig. 1. $2^{nd}$-order harmonic event plane angle resolution ($\sqrt{\cos[2(\psi_2^A - \psi_2^B)]}$) as a function of centrality.

where, $\psi_2^A$ and $\psi_2^B$ are the event plane angles in the sub-events A and B, respectively.

Figure 1 shows the event plane resolution as a function of centrality at mid-rapidity ($|\eta| < 1.0$) in Ru+Ru and Zr+Zr collisions at $\sqrt{s_{\rm NN}} = 200$ GeV. For comparison, event plane resolution from the published results in Au+Au collisions at $\sqrt{s_{\rm NN}} = 200$ GeV and U+U collisions at $\sqrt{s_{\rm NN}} = 193$ GeV are also shown. The event plane resolution improves with the increase in multiplicity of the systems and the number of participating nucleons for a given centrality. Furthermore, a similar trend in centrality dependence is observed across all examined collision systems.

## 3. Results

### 3.1. $p_T$ dependence of $v_2$

Figure 2 presents the $v_2$ of strange and multi-strange hadrons as a function of $p_T$ in minimum bias (0-80%) Ru+Ru and Zr+Zr collisions at $\sqrt{s_{\rm NN}} = 200$ GeV. A distinct mass ordering of $v_2$ at lower $p_T$ indicate hydrodynamic nature of the medium produced in these collisions. A splitting between baryons and mesons $v_2$ at intermediate $p_T$ suggests that constituent quarks contribute to their $v_2$. This indicates the formation of a QGP medium during isobar collisions at $\sqrt{s_{\rm NN}} = 200$ GeV. A similar transverse momentum dependence of $v_2$ is observed in both Ru+Ru and Zr+Zr collisions.

Figure 2 also shows $v_2$ of strange and multi-strange hadrons scaled by the number of constituent quarks $n_q$ in minimum bias Ru+Ru and Zr+Zr collisions at $\sqrt{s_{\rm NN}}$ = 200 GeV. The results are presented as a function of transverse kinetic energy to remove the effect of particle mass at low $p_T$. It is defined as $KE_T = m_T - m_0$, where $m_T$ is the transverse mass ($\sqrt{p_T^2 + m_0^2}$) and $m_0$ is rest mass of the particle. The $v_2$ of strange and multi-strange hadrons follows the number of constituent quarks (NCQ) scaling within ±15% in both collision systems. This also suggests that the

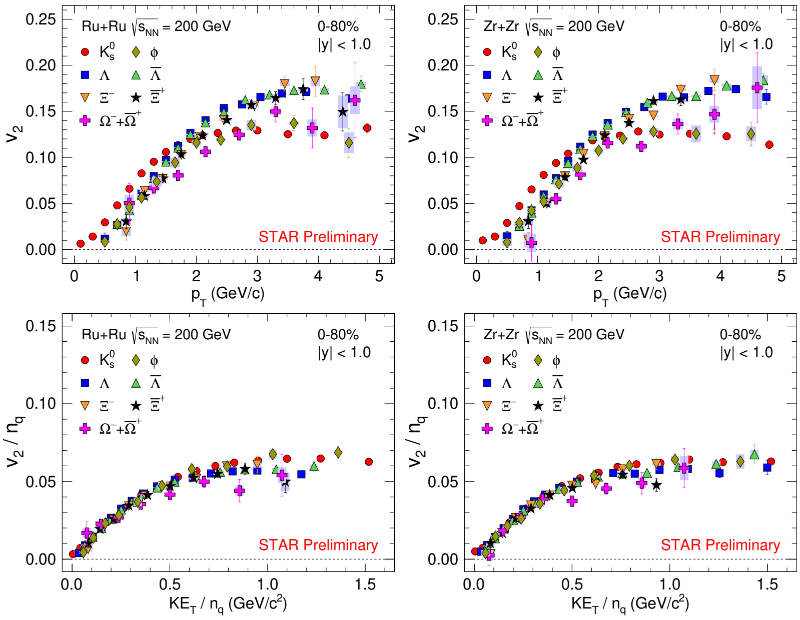


Fig. 2. (top panels) $v_2$ as a function of $p_T$ for $K_s^0$, $\Lambda$, $\bar{\Lambda}$, $\phi$, $\Xi^-$, $\overline{\Xi}^+$, and $\Omega^-$+$\overline{\Omega}^+$ at mid-rapidity in minimum bias Ru+Ru and Zr+Zr collisions at $\sqrt{s_{\mathrm{NN}}}$ = 200 GeV. (bottom panels) NCQ scaled $v_2$ vs transverse kinetic energy ($KE_T/n_q$) is also shown for Ru+Ru and Zr+Zr collisions at $\sqrt{s_{\mathrm{NN}}}$ = 200 GeV. The bands represent systematic uncertainties.

dominant mechanism of particle production is quark coalescence.

### 3.2. *Centrality dependence of $v_2$*

Figures 3 shows $v_2(p_T)$ of strange hadrons for various centrality intervals in Ru+Ru and Zr+Zr collisions at $\sqrt{s_{\mathrm{NN}}}$ = 200 GeV. A strong centrality dependence is observed for all the particles studied in both the isobar systems. The magnitude of $v_2$ increases from central (0-10%) to peripheral (40-80%) collisions, which indicate the effect of initial eccentricity in isobar collisions at $\sqrt{s_{\mathrm{NN}}}$ = 200 GeV.

Figure 4 shows $p_T$-integrated $v_2$ of strange hadrons as a function of centrality in Ru+Ru and Zr+Zr collisions at $\sqrt{s_{\mathrm{NN}}}$ = 200 GeV. The ratio of $v_2$ in Ru+Ru to Zr+Zr collisions is also shown in the bottom panels of Fig. 4 and fitted with a constant polynomial function for mid-central collisions (20-50%). About ∼2% deviation from unity with a significance of 6.25$\sigma$ for $\Lambda(\bar{\Lambda})$ and 1.83$\sigma$ for $K_s^0$ is observed. This deviation aligns with the theoretical expectations based on the differences in the nuclear structures of the two isobaric nuclei.[16]

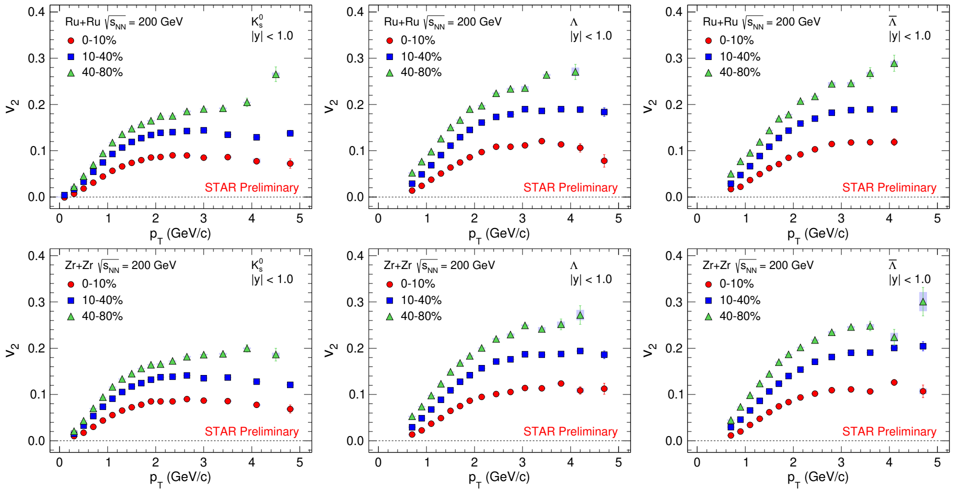


Fig. 3. $v_2(p_T)$ of strange hadrons at mid-rapidity in Ru+Ru (top panels) and Zr+Zr (bottom panels) collisions at $\sqrt{s_{NN}}$ = 200 GeV for centrality 0-10%, 10-40%, and 40-80%. The bands represent systematic uncertainties.

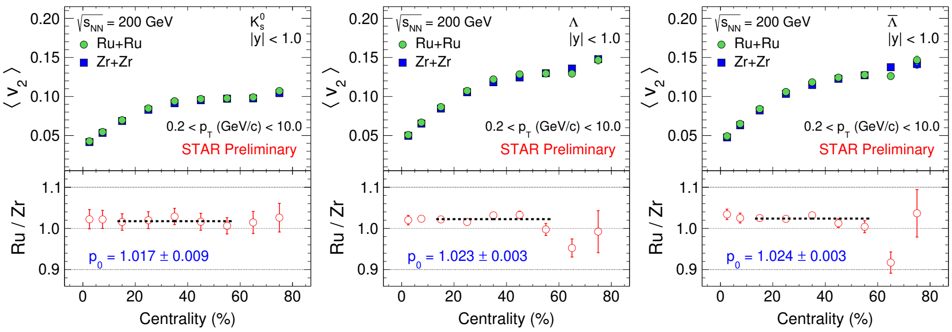


Fig. 4. $p_T$-integrated $v_2$ vs centrality for strange hadrons at mid-rapidity in Ru+Ru and Zr+Zr collisions at $\sqrt{s_{NN}}$ = 200 GeV. The bottom panels also show the ratio of $v_2$ between Ru and Zr. The error bars represent statistical and systematic uncertainties added in quadrature.

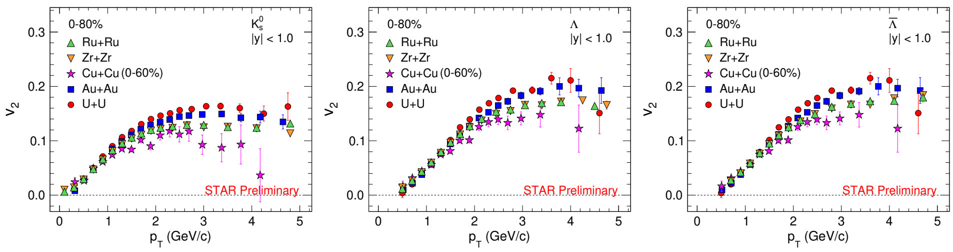


Fig. 5. Strange hadron $v_2$ as a function of $p_T$ at mid-rapidity in minimum bias Ru+Ru and Zr+Zr collisions at $\sqrt{s_{NN}}$ = 200 GeV compared to Cu+Cu, Au+Au, and U+U collisions.[17–19] The error bars represent statistical and systematic uncertainties added in quadrature.

### 3.3. *System size dependence*

Figure 5 shows $v_2$ of strange hadrons in Ru+Ru and Zr+Zr collisions at $\sqrt{s_{\rm NN}}$ = 200 GeV compared to the published results from the STAR experiment at RHIC in Cu+Cu, Au+Au, and U+U collisions.[17–19] For $p_T$ values above ∼1.5 GeV/$c$, the value of $v_2$ appears to depend on the size of the system. Notably, the $v_2$ values follow a clear order: $v_2^{\rm Cu} < v_2^{\rm Ru/Zr} < v_2^{\rm Au} < v_2^{\rm U}$, indicating that the magnitude of $v_2$ increases with an increase in system size.

### 3.4. *Model comparison*

The AMPT model is a Monte Carlo event generator extensively used to study relativistic heavy-ion collisions.[20] The colliding nuclei in AMPT are modeled according to a deformed Wood-Saxon distribution with nuclear radius given by,

$$R(\theta, \phi) = R_0 \left[1 + \beta_2 Y_{2,0}(\theta, \phi) + \beta_3 Y_{3,0}(\theta, \phi)\right]. \tag{3}$$

$R_0$ represents the radius parameter, $\beta_2$ and $\beta_3$ are the quadrupole and octupole deformities, and $Y_{l,m}(\theta, \phi)$ are the spherical harmonics. We studied two different cases of Wood-Saxon parameters for Ru+Ru and Zr+Zr collisions at $\sqrt{s_{\rm NN}}$ = 200 GeV, as shown in Table 1.[21] For each case, we analyzed approximately 9 million minimum bias events for Ru+Ru and Zr+Zr collisions at $\sqrt{s_{\rm NN}}$ = 200 GeV with a parton-parton cross-section of 3 mb.

Table 1. Parameter set for various deformation configurations of the Ru and Zr nuclei in the AMPT model

| **Parameter** | **Default** | | **Deformed** | |
|---|---|---|---|---|
| System | Ru | Zr | Ru | Zr |
| $R_0$ | 5.096 | 5.096 | 5.090 | 5.090 |
| $a$ | 0.540 | 0.540 | 0.460 | 0.520 |
| $\beta_2$ | 0.000 | 0.000 | 0.162 | 0.060 |
| $\beta_3$ | 0.000 | 0.000 | 0.000 | 0.200 |

Figure 6 and 7 show $v_2$ of strange and multi-strange hadrons in minimum bias Ru+Ru and Zr+Zr collisions at $\sqrt{s_{\rm NN}}$ = 200 GeV compared to the AMPT-SM model calculations. The AMPT-SM model with or without deformation appears to be in good agreement with each other, and both the models agree with the data in the measured $p_T$ range for minimum-bias isobar collisions at $\sqrt{s_{\rm NN}}$ = 200 GeV.

## 4. Summary

We have reported transverse momentum dependence of elliptic flow of $K_s^0$, $\Lambda$, $\bar{\Lambda}$, $\phi$, $\Xi^-$, $\overline{\Xi}^+$, and $\Omega^-$+$\overline{\Omega}^+$ at mid-rapidity in Ru+Ru and Zr+Zr collisions at $\sqrt{s_{\rm NN}}$

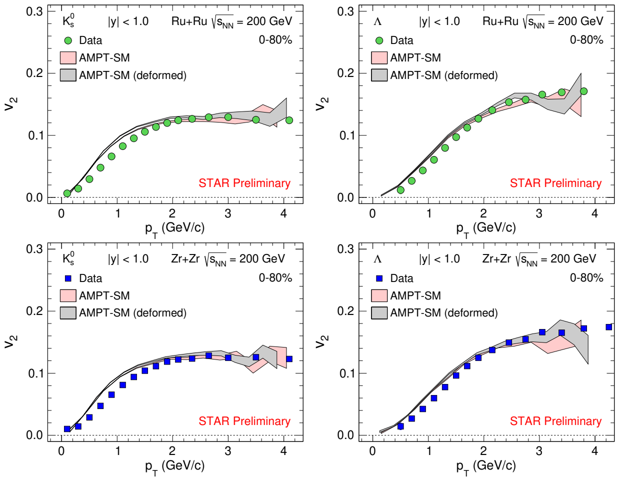


Fig. 6. $v_2$ as a function of $p_T$ for strange hadrons ($K_s^0$, Λ, and $\bar{\Lambda}$) at mid-rapidity in minimum bias Ru+Ru and Zr+Zr collisions at $\sqrt{s_{\rm NN}} = 200$ GeV compared to the AMPT model calculations.[20,21] The error bars represent statistical and systematic uncertainties added in quadrature.

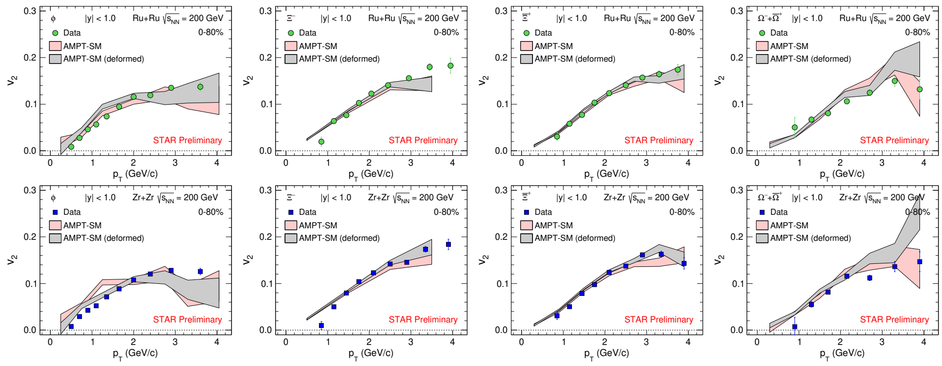


Fig. 7. $v_2$ as a function of $p_T$ for multi-strange hadrons ($\phi$, $\Xi^-$, $\overline{\Xi}^+$, and $\Omega^-$+$\overline{\Omega}^+$) at mid-rapidity in minimum bias Ru+Ru and Zr+Zr collisions at $\sqrt{s_{\rm NN}} = 200$ GeV compared to the AMPT model calculations.[20,21] The error bars represent statistical and systematic uncertainties added in quadrature.

= 200 GeV for minimum bias (0-80%) and in three centrality intervals (0-10%, 10-40%, and 40-80%). We observed a particle mass hierarchy of $v_2$, which suggests hydrodynamic behavior at low $p_T$. We also observed a baryon-meson splitting of $v_2$ at intermediate $p_T$. Furthermore, the elliptic flow of strange and multi-strange hadrons follows the number of constituent quark scaling, providing further evidence for quark coalescence as the dominant particle production mechanism and the collectivity of the medium.

A clear centrality dependence of $v_2$ is observed in the isobar collisions. The ratio of $p_T$-integrated $v_2$ for strange hadrons between the two isobar collisions shows a deviation from unity, indicating different intrinsic nuclear structures of the two isobars. Furthermore, We also observed a system size dependence of the $v_2$ above $p_T > 1.5$ GeV/$c$. The AMPT-SM model, with and without nuclear deformation, provides a good description of the data within the measured $p_T$ range for minimum-bias isobar collisions at $\sqrt{s_{\rm NN}} = 200$ GeV. These measurements provide insight into the impact of collision geometry and nuclear deformation on the anisotropic flow of particles in relativistic heavy-ion collisions.

## 5. Bibliography

## References

1. E. V. Shuryak, *Phys. Lett. B* **78**, 150-153 (1978).
2. J. Cleymans, R. V. Gavai, E. Suhonen, *Phys. Rep.* **130**, 217-292 (1986).
3. F. Karsch, *Nucl. Phys. A* **698**, 199-208 (2002).
4. I. Arsene *et al.* (BRAHMS Collaboration), *Nucl. Phys. A* **757**, 1-27 (2005).
5. B. B. Back *et al.* (PHOBOS Collaboration), *Nucl. Phys. A* **757**, 28-101 (2005).
6. J. Adams *et al.* (STAR Collaboration), *Nucl. Phys. A* **757**, 102-183 (2005).
7. K. Adcox *et al.* (PHENIX Collaboration), *Nucl. Phys. A* **757**, 184-283 (2005).
8. K. Aamodt *et al.* (ALICE Collaboration), *Phys. Rev. Lett.* **105**, 252302 (2010).
9. G. Aad *et al.* (ATLAS Collaboration), *Phys. Lett. B* **707**, 330-348 (2012).
10. S. Chatrchyan *et al.* (CMS Collaboration), *Phys. Rev. C* **87**, 014902 (2013).
11. A. M. Poskanzer, S. A. Voloshin, *Phys. Rev. C* **58**, 1671 (1998).
12. S. A. Bass *et al. J. Phys. G* **25**, R1-R57 (1999).
13. M. S. Abdallah *et al.* (STAR Collaboration) *Phys. Rev. C* **105**, 014901 (2022).
14. J. Adams *et al.* (STAR Collaboration) *Phys. Rev. Lett.* **95**, 122301 (2005).
15. L. Adamczyk *et al.* (STAR Collaboration) *Phys. Rev. C* **88**, 014902 (2013).
16. M. S. Abdallah *et al.* (STAR Collaboration), *Phys. Rev. C* **105**, 014901 (2022).
17. B. I. Abelev *et al.* (STAR Collaboration), *Phys. Rev. C* **77**, 054901 (2008).
18. B. I. Abelev *et al.* (STAR Collaboration), *Phys. Rev. C* **81**, 044902 (2010).
19. M. S. Abdallah *et al.* (STAR Collaboration), *Phys. Rev. C* **103**, 064907 (2021).
20. Z.-W. Lin *et al. Phys. Rev. C* **72**, 064901 (2005).
21. P. Sinha *et al. Phys. Rev. C* **108**, 024911 (2023).